Chemotaxis of Cargo-Carrying Self-Propelled Particles

Hidde D. Vuijk,[1] Holger Merlitz,[1] Michael Lang,[1] Abhinav Sharma,[1,2,*] and Jens-Uwe Sommer[1,2,†]
[1]*Leibniz-Institut für Polymerforschung Dresden, Institut Theory der Polymere, 01069 Dresden, Germany*
[2]*Technische Universität Dresden, Institut für Theoretische Physik, 01069 Dresden, Deutschland*

(Received 28 October 2020; accepted 23 April 2021; published 21 May 2021)

Active particles with their characteristic feature of self-propulsion are regarded as the simplest models for motility in living systems. The accumulation of active particles in low activity regions has led to the general belief that chemotaxis requires additional features and at least a minimal ability to process information and to control motion. We show that self-propelled particles display chemotaxis and move into regions of higher activity if the particles perform work on passive objects, or cargo, to which they are bound. The origin of this cooperative chemotaxis is the exploration of the activity gradient by the active particle when bound to a load, resulting in an average excess force on the load in the direction of higher activity. Using a new theoretical model, we capture the most relevant features of these active-passive dimers, and in particular we predict the crossover between antichemotactic and chemotactic behavior. Moreover, we show that merely connecting active particles to chains is sufficient to obtain the crossover from antichemotaxis to chemotaxis with increasing chain length. Such an active complex is capable of moving up a gradient of activity such as provided by a gradient of fuel and to accumulate where the fuel concentration is at its maximum. The observed transition is of significance to protoforms of life, enabling them to locate a source of nutrients even in the absence of any supporting sensomotoric apparatus.

DOI: 10.1103/PhysRevLett.126.208102

Escherichia coli is able to steer toward sources of nutrients by altering its tumble rate [1]. While searching, it performs temporal comparisons of nutrient concentrations along its trajectory, and as the concentration increases, the swimmer lowers its tumble rate to move up the concentration gradient of nutrients. This search strategy, known as "klinokinesis with adaption," leads to accumulation of bacteria near the top of the nutrient density and thus to chemotaxis [2,3]. It requires a delicate apparatus for chemical sensing and information processing and a corresponding motoric response, available only to organisms that have reached an advanced level of evolution.

Much simpler are self-propelled particles, which merely adjust their speed in response to the *local* fuel concentration, a mechanism called "orthokinesis." Synthetic Janus particles, an example of this class of swimmers, are driven by catalytic reactions in the presence of, e.g., hydrogen peroxide [4] or hydrazine [5]. Biological molecules such as catalytic enzymes have also been reported to show orthokinetic behavior [6]. Instead of intentional tumble movements, induced by flagella as used by E. coli, these particles change direction randomly through rotational Brownian motion, and, if of roughly spherical shape, the rotational relaxation time is almost independent of the degree of propulsion. Usually, their swim speed (i.e., degree of activity) is positively correlated with the concentration of fuel. As a consequence, one can show that in the presence of a fuel gradient such active Brownian particles (ABPs) accumulate in regions where the fuel concentration is low, known as antichemotactic behavior [7,8]. This corresponds qualitatively to that of passive Brownian particles in a temperature gradient [9] and to everyday experience that physical bodies accumulate in regions where they are less agitated or moved. This has been recently shown to play a role in the positioning of the nucleus in certain animal cells [10–12]. Although ABPs can display interesting transient behavior in fuel gradients, called pseudochemotaxis [13–16], activity does not lead to an advantage in the search for fuel sources compared to passive diffusion on long timescales [17].

These observations have led to the general belief that chemotaxis, a prominent feature of living systems, cannot be reflected by uninformed moving objects, in particular not by ABPs. In this Letter, we demonstrate that ABPs can show chemotactic behavior in activity gradients when they are bound to a passive cargo particle. With increasing cargo, the active-passive complex switches its behavior from antichemotactic to chemotactic and accumulates in regions with a large fuel concentration (see Fig. 1). Furthermore, we show that an explicit distinction between cargo and active particles is not fundamental to our proposed mechanism and can self-emerge in an active system. We demonstrate this in a system of ABPs connected in a chain: with increasing chain length, there is a crossover from antichemotaxis to chemotaxis.

Our model consists of an ABP [18] attached to a passive cargo by a stiff bond, thus forming a dimer. The activity of

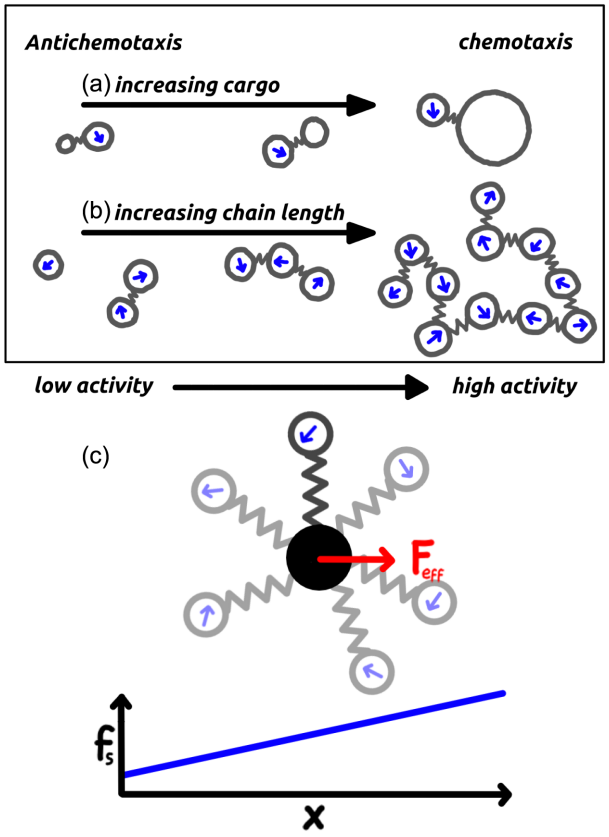

FIG. 1. Crossover from antichemotactic to chemotactic behavior. ABPs are sketched as circles with arrows. Cargo particles (sketched as empty circles) are bound to ABPs. (a) When the cargo is small, that is, its friction coefficient is small, the dimer accumulates in low activity regions (antichemotaxis). When the cargo is large, the dimer accumulates in the high activity regions (chemotaxis). (b) Self-emergence of cargo in active chains. When active particles are connected in a chain, one observes the crossover from antichemotactic to chemotactic behavior with increasing chain length. (c) A sketch of the Born-Oppenheimer approximation. A single ABP is connected to a cargo (black circle) with a fixed position. Because the cargo is fixed in space, the ABP (open circle with arrow) is able to explore the space around the cargo (translucent ABPs) and sense the gradient in the swim force (f_s). On average, the ABP pulls on the cargo in the direction of the gradient of the swim force, which results in an effective force (F_{eff}) on the cargo. The f_s/x graph in (c) shows the swim force in the neighborhood of the cargo.

the ABP is characterized by its persistence time τ (characteristic time of rotation of the active particle) and a space-dependent swim force $f_s(\boldsymbol{r})$, which we assume to be proportional to the local fuel concentration. Regions where the swim force is large (small) we call high (low) activity regions. The friction coefficient of the ABP is γ and that of the cargo is $q\gamma$. The load on the ABP is increased by increasing q. Temperature is denoted by T in units of the Boltzmann constant.

The Fokker-Planck equation corresponding to the probability density of this system is

$$\begin{aligned}\partial_t P(t) = &-\frac{1}{\gamma}\nabla_1 \cdot [\boldsymbol{F}P(t) + f_s \boldsymbol{p} P(t) - T\nabla_1 P(t)] \\ &+ \frac{1}{q\gamma}\nabla_2 \cdot [\boldsymbol{F}P(t) + T\nabla_2 P(t)] \\ &+ \frac{1}{(d-1)\tau}\mathcal{R}^2 P(t), \end{aligned} \tag{1}$$

where $P(t) = P(\boldsymbol{r}_1, \boldsymbol{p}, \boldsymbol{r}_2, t)$, $\boldsymbol{r}_1$ and $\boldsymbol{p}$ are the position and orientation of the ABP, $\boldsymbol{r}_2$ is the position of the passive particle, and t is the time. The force $\boldsymbol{F}$ comes from the stiff bond with unit length connecting the two particles. $\mathcal{R} = \boldsymbol{p} \times \nabla_p$ is the rotation operator [19]. All results hold for $d \in \{2, 3\}$ dimensions.

We coarse grain Eq. (1) in two steps. First, we expand $P(t)$ in eigenfunctions of $\mathcal{R}^2$ [20–24] and transform to the "center-of-friction" coordinate $\boldsymbol{R} = (1/1+q)\boldsymbol{r}_1 + (q/1+q)\boldsymbol{r}_2$, which we take as the position of the dimer, and the internal coordinate $\boldsymbol{r}' = \boldsymbol{r}_1 - \boldsymbol{r}_2$. Then we integrate out the orientational degrees of freedom $\boldsymbol{p}$ and the internal coordinate and ignore terms $\mathcal{O}(\nabla^3)$ [25]. This approximation is valid when the separation between the ABP and the passive particle and the persistence length of the ABP are small compared to gradients in the system. This results in the following equation for the probability density of the dimer:

$$\partial_t \rho(\boldsymbol{R}, t) = -\nabla \cdot \boldsymbol{J}, \tag{2}$$

where the flux of the dimers is

$$\boldsymbol{J} = -\frac{1}{2}\epsilon\rho(\boldsymbol{R}, t)\nabla D(\boldsymbol{R}) - D(\boldsymbol{R})\nabla\rho(\boldsymbol{R}, t), \tag{3}$$

with

$$\epsilon = 1 - q\frac{d-1}{d}, \tag{4}$$

and

$$D(\boldsymbol{R}) = \frac{1}{1+q}\frac{T}{\gamma} + \frac{1}{(1+q)^2}\frac{\tau}{d\gamma^2} f_s^2(\boldsymbol{R}), \tag{5}$$

is the coarse-grained space-dependent diffusion coefficient of the dimer. The theoretical results are validated by Brownian dynamics simulations [37,38]. Details of the simulations can be found in the Supplemental Material [25].

Figure 2 shows the stationary density distribution of dimers with a different friction ratio q. As long as the cargo is highly mobile (small q), the dimer accumulates in regions of low activity like a single ABP, which—being an orthokinetic swimmer—is antichemotactic. When the cargo has large friction (large q), it exhibits chemotaxis and accumulates where the activity is high. The crossover from antichemotactic to chemotactic behavior is captured by the

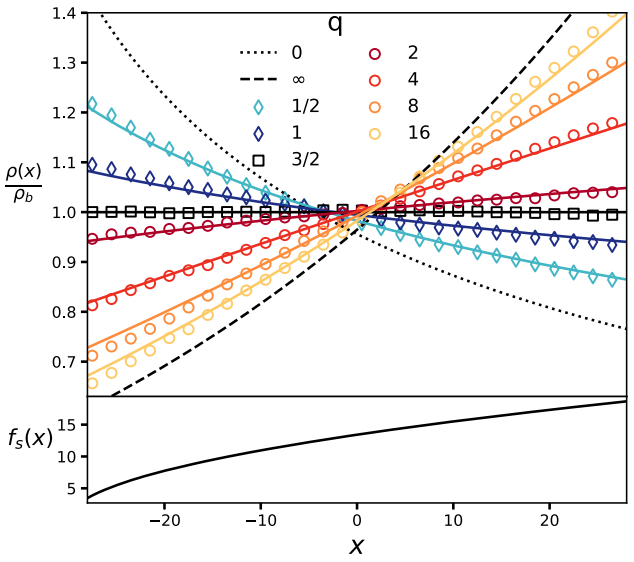

FIG. 2. Density distributions of ABPs relative to the bulk density $\rho_b = \frac{1}{56}\int_{-28}^{28} dx\rho(x)$ in three dimensions rigidly bound to a passive cargo particle with different friction (top panel). The bond length of the dimer is unity and is used as the unit of length. The ABP has an orientational correlation time of $\tau = 1/40$ and a swim force $f_s(x) = \sqrt{6(x+30)}$ (bottom panel). The dimensions of the simulation box are $60 \times 60 \times 60$. The particles interact with the confining walls via a short-range Weeks-Chandler-Anderson potential [39]. Because the theory ignores boundary effects, we only show the density for $-28 < x < 28$. Boundary effects could be included using the methods described in [40,41]. Symbols show simulation results; solid lines show the analytical prediction [Eq. (6)]. With a highly mobile cargo particle (blue diamonds), the dimer accumulates in regions of low activity (antichemotaxis). At the predicted friction ratio $q = d/(d-1) = 3/2$, a uniform concentration is found (black squares). With a less mobile cargo (circles), the dimer accumulates where the activity is high (chemotaxis). The dashed line shows the limit of infinite friction of the cargo. This limiting case corresponds to the behavior of the system under the Born-Oppenheimer approximation in which the cargo particle can be considered as immobile and the ABP moving in a stationary potential. The dotted line shows the limit of vanishing friction of the cargo, where the dimer behaves like a single ABP.

coarse-grained equations, which yield the following expression for the steady-state density of the dimer:

$$\rho(\boldsymbol{R}) \propto \left[1 + \frac{1}{1+q}\frac{\tau}{\gamma T d} f_s^2(\boldsymbol{R})\right]^{-\frac{1}{2}\epsilon}. \tag{6}$$

For $q < d/(d-1)$, ϵ is positive, and the dimer is chemotactic. For $q > d/(d-1)$, ϵ is negative, and the dimer is antichemotactic. At the threshold $q = d/(d-1)$, the distribution of the dimer is uniform and independent of the swim force. Note that, in the limit of $q \to 0$, the density distribution of the dimer reduces to that of a single ABP, and it accumulates in the region of low activity. In general, the exponent ϵ depends on the potential between the two particles. In the Supplemental Material, we show that the qualitative behavior of the system is unaffected by the choice of the potential [25].

In order to understand the mechanism behind the switch from antichemotaxis to chemotaxis for increasing q, we consider the small and large q limits separately. When the friction coefficient of the cargo particle is much smaller than that of the ABP, the cargo relaxes to its quasisteady state distribution at each position of the ABP. In this limit, one can consider the dimer to be a single ABP with an increased friction coefficient. Accordingly, the dimer accumulates in the low activity regions (antichemotaxis). In the limit of large friction of the cargo particle, the ABP relaxes to a quasisteady state distribution at each position of the load particle, and the ABP probes the neighborhood of the cargo particle. The activity gradient results in an effective force on the cargo particle in the direction of the activity gradient. In this limit, one observes the accumulation of the system in high activity regions (chemotaxis).

The steady-state density in the large friction limit can be obtained following an independent approach similar to the Born-Oppenheimer approximation in quantum mechanics [42]. When the cargo is large, one can consider it as immobile and the ABP as moving in a stationary potential. The ABP explores the environment around the load and exerts an effective force

$$\boldsymbol{F}_{\text{eff}}(\boldsymbol{r}_2) = \frac{d-1}{d}\frac{\tau}{2d\gamma}\nabla_2 f_s^2(\boldsymbol{r}_2) \tag{7}$$

on it, which is up the swim force gradient (see Fig. 1). This effective force can be considered as the driving force for the total system. The steady-state density of a passive Brownian particle with friction $q\gamma$ in a such an effective force field is

$$\rho(\boldsymbol{R}) \propto \exp\left[\frac{1}{T}\frac{d-1}{d}\frac{\tau}{2d\gamma} f_s^2(\boldsymbol{R})\right], \tag{8}$$

which shows that for large q the dimer moves preferentially to regions of high fuel concentration. For details of the calculations, see the Supplemental Material [25]. Note that this density is the $q \to \infty$ limit of Eq. (6). This consideration shows that it is indeed the ability of the active particle to explore the activity gradient that causes the chemotaxis.

Whereas the steady-state distribution measures the chemotactic behavior of the dimer, it does not shed light on the "efficiency" of the chemotactic transport of cargo particles by the ABPs. Though large q results in the strongest chemotactic behavior, it also slows down the transport of the cargo particle due to the increased friction of the dimer. In our case, this leads to an optimum q that yields the fastest transport to regions of high activity. To quantify this, we use the initial rate of change of the average

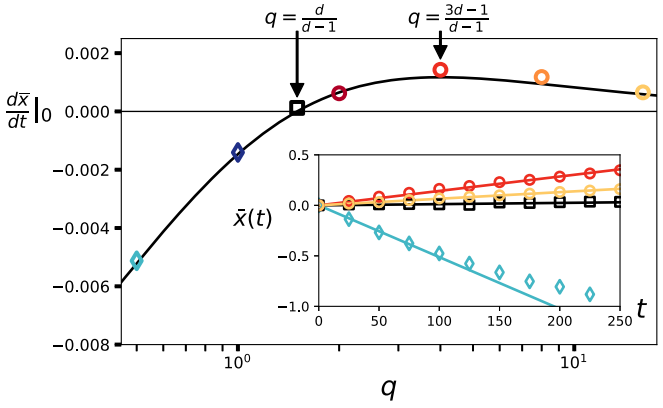

FIG. 3. Time derivative at $t = 0$ of the average position of the dimer in the same setup as Fig. 2, starting with a uniform distribution ($d\bar{x}/dt$). Symbols show simulation results (colors as in Fig. 2). The line is the theoretical prediction $d\bar{x}/dt \propto \epsilon/(1+q)^2$ with the proportionality constant fitted to the data (for details, see [28]). Inset: initial time evolution of the average position $[x(t)]$ for several values of q. The solid lines show the linear fit for the short time from which the data in the main figure is extracted. For $q < d/(d-1) = 3/2$, the dimers move to the left down the swim force gradient. For $q > 3/2$, the dimers move to the right up the swim force gradient. As q increases beyond $(3d-1)/(d-1) = 4$, the dynamics start to slow down due to the increase in the friction of the dimer.

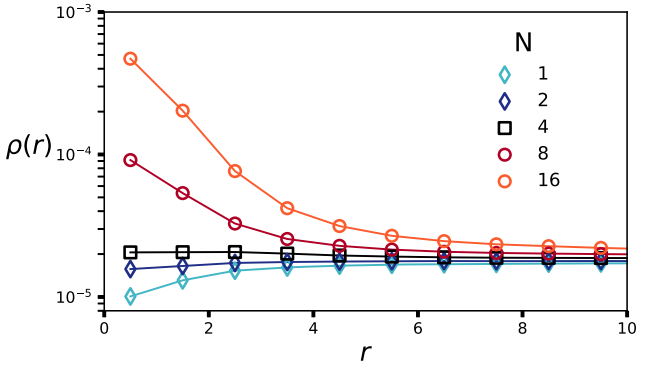

FIG. 4. Stationary concentrations of ABP molecules inside a spherical container of radius $r_{\max} = 25$. The symbols show simulation data, and the lines are a guide for the eye. The source of the activity is at the center of the container, and the driving force decreases as $f_s(r) = 15/r$ for $r \geq 1$ and remains constant $f_s(r) = 15$ for $r < 1$. This activity profile corresponds to a stationary fuel source emitting fuel by diffusion. The single particles and dimers are antichemotactic and are driven out of the region of high activity (blue diamonds) The quadromer is distributed uniformly (black squares). Longer polymers ($N > 4$, red circles) are chemotactic and accumulate near the peak of the fuel concentration.

position of the dimer, starting with a uniform distribution (see Fig. 3). For this setup, the displacement of the dimer is determined by the convective velocity, which can be read off from Eq. (3), $\boldsymbol{V}(\boldsymbol{R}) = -\frac{1}{2}\epsilon\nabla D(\boldsymbol{R}) \propto \nabla f_s^2 \epsilon/(1+q)^2$. Depending on the value of q, this is either up the swim force gradient (chemotaxis) or down the swim force gradient (antichemotaxis). The convective velocity has a maximum at $q = (3d-1)/(d-1)$, which coincides with the simulation result. Note that for biased movement up the swim force gradient, only a large enough cargo is necessary, and no memory [43], temporal integration of the fuel concentration [44], or an explicit coupling between the swim force gradient and the orientation of the ABP [45,46] is required.

Instead of coupling an ABP to a passive cargo, several ABPs can be combined to form chains or clusters of N "monomers" [47,48]. Then, each individual ABP may be regarded as an active pulling agent connected to a "cargo" of $N-1$ particles because the other $N-1$ ABPs do not pull coherently in identical directions but rather in random directions. Figure 4 displays the stationary radial density distribution profiles of the molecules inside the container. Short oligomers are antichemotactic and stay away from regions of high activity. Long polymers, on the other hand, are chemotactic and accumulate where activity is high. The crossover point is seen with the quadromer, which is roughly uniformly distributed in the activity field.

Polymeric ABPs are therefore qualitatively similar to a single ABP coupled to a passive cargo. If either the cargo is sufficiently inert or the degree of polymerization sufficiently high, such that it inhibits the free motion of an individual ABP, then the situation of a single ABP inside an approximately stationary potential arises. Inside an activity gradient, the particle is running up the confining potential in the direction of increasing activity. This bias generates a net force which, if the system is mobile, drives the same up the activity gradient. If, however, the cargo is rather mobile, then the motion of the ABP remains approximately undisturbed and the complex runs down the activity gradient as an individual ABP does.

ABPs are equivalent to other models of active matter, such as run-and-tumble particles [20,49] or active Ornstein-Uhlenbeck particles [50,51], and the results shown here also apply to these models. We show in the Supplemental Material [25] that the chemotactic behavior observed in the active-passive dimer cannot be reproduced in a system of dimers in which the active particle is replaced by a passive Brownian particle coupled to a spatially inhomogeneous thermostat [25].

An interesting outlook is the development of artificial nanomachines that can locate origins of fuel gradients based on the design principle of coupling ABPs to passive cargo without a complex sensing and steering system. Furthermore, a natural progression of this work is to study how the behavior of a single active-passive dimer or more complex clusters in an activity gradient affect the collective properties of a system with a large number of such components [52–55].

The coupling of active bodies with or without passive bodies leads to effective sensing of gradients of activity (fuel) and can be generalized in several directions. First, the connectivity between the bodies does not need to be linear as in the studies presented in this Letter. Virtually any kind of topology of connecting the active bodies leads to effective chemotaxis, given that the complex provides sufficient friction to single active bodies. Moreover, active bodies moving inside a container that is permeable for the fuel but not for the active bodies can give rise to chemotactic motion of the container, provided the activity gradient is present inside the container. Also in this case, it is the exploration of the active bodies in the gradient field that leads to a higher averaged pressure on the container walls located at the higher activity. Our results may shed light on the origin of prebiotic forms of life and how chemotactic sensing has emerged during evolution.

A. S. acknowledges support by the Deutsche Forschungsgemeinschaft (DFG) within the Project No. SH 1275/3-1. J. U. S. thanks the cluster of excellence "Physics of Life" at TU Dresden for its support. We thank B. M. Friedrich for a critical reading of the manuscript.

*Corresponding author.
sharma@ipfdd.de
†Corresponding author.
sommer@ipfdd.de

[1] H. C. Berg, *E. coli in Motion* (Springer Verlag, Heidelberg, Germany, 2004).
[2] M. J. Schnitzer, S. M. Block, H. C. Berg, and E. M. Purcell, Strategies for chemotaxis, Symp. Soc. Gen. Microbiol. **46**, 15 (1990).
[3] H. C. Berg, *Random Walks in Biology* (Princeton University Press, Chichester, West Sussex, 1993).
[4] J. R. Howse, R. A. L. Jones, A. J. Ryan, T. Gough, R. Vafabakhsh, and R. Golestanian, Self-Motile Colloidal Particles: From Directed Propulsion to Random Walk, Phys. Rev. Lett. **99**, 048102 (2007).
[5] W. Gao, A. Pei, R. Dong, and J. Wang, Catalytic iridium-based janus micromotors powered by ultralow levels of chemical fuels, J. Am. Chem. Soc. **136**, 2276 (2014).
[6] A.-Y. Jee, S. Dutta, Y.-K. Cho, T. Tlusty, and S. Granick, Enzyme leaps fuel antichemotaxis, Proc. Natl. Acad. Sci. U.S.A. **115**, 14 (2018).
[7] M. J. Schnitzer, Theory of continuum random walks and application to chemotaxis, Phys. Rev. E **48**, 2553 (1993).
[8] A. Sharma and J. M. Brader, Brownian systems with spatially inhomogeneous activity, Phys. Rev. E **96**, 032604 (2017).
[9] N. G. van Kampen, Diffusion in inhomogeneous media, Z. Phys. B **68**, 135 (1987).
[10] M. Almonacid, W. W. Ahmed, M. Bussonnier, P. Mailly, T. Betz, R. Voituriez, N. S. Gov, and M.-H. Verlhac, Active diffusion positions the nucleus in mouse oocytes, Nat. Cell Biol. **17**, 470 (2015).
[11] N. Razin, R. Voituriez, J. Elgeti, and N. S. Gov, Generalized Archimedes' principle in active fluids, Phys. Rev. E **96**, 032606 (2017).
[12] N. Razin, R. Voituriez, J. Elgeti, and N. S. Gov, Forces in inhomogeneous open active-particle systems, Phys. Rev. E **96**, 052409 (2017).
[13] I. R. Lapidus, 'pseudochemotaxis' by micro-organisms in an attractant gradient, J. Theor. Biol. **86**, 91 (1980).
[14] F. Peng, Y. Tu, J. C. M. van Hest, and D. A. Wilson, Self-guided supramolecular cargo-loaded nanomotors with chemotactic behavior towards cells, Angew. Chem. **127**, 11828 (2015).
[15] P. K. Ghosh, Y. Li, F. Marchesoni, and F. Nori, Pseudochemotactic drifts of artificial microswimmers, Phys. Rev. E **92**, 012114 (2015).
[16] H. D. Vuijk, A. Sharma, D. Mondal, J.-U. Sommer, and H. Merlitz, Pseudochemotaxis in inhomogeneous active brownian systems, Phys. Rev. E **97**, 042612 (2018).
[17] H. Merlitz, H. D. Vuijk, R. Wittmann, S. Abhinav, and J.-U. Sommer, Pseudo-chemotaxis of active Brownian particles competing for food, PLoS One **15**, e0230873 (2020).
[18] C. Bechinger, R. Di Leonardo, H. Löwen, C. Reichhardt, G. Volpe, and G. Volpe, Active particles in complex and crowded environments, Rev. Mod. Phys. **88**, 045006 (2016).
[19] P. M. Morse and H. Feshbach, *Methods of Theoretical Physics* (McGraw-Hill, New York, 1953), Vol. 1.
[20] M. E. Cates and J. Tailleur, When are active Brownian particles and run-and-tumble particles equivalent? consequences for motility-induced phase separation, Europhys. Lett. **101**, 20010 (2013).
[21] A. Duzgun and J. V. Selinger, Active Brownian particles near straight or curved walls: Pressure and boundary layers, Phys. Rev. E **97**, 032606 (2018).
[22] A. P. Solon, M. E. Cates, and J. Tailleur, Active Brownian particles and run-and-tumble particles: A comparative study, Eur. Phys. J. Spec. Top. **224**, 1231 (2015).
[23] H. D. Vuijk, J.-U. Sommer, H. Merlitz, J. M. Brader, and A. Sharma, Lorentz forces induce inhomogeneity and flux in active systems, Phys. Rev. Research **2**, 013320 (2020).
[24] M. T. Vrugt and R. Wittkowski, Relations between angular and cartesian orientational expansions, AIP Adv. **10**, 035106 (2020).
[25] See Supplemental Material at http://link.aps.org/supplemental/10.1103/PhysRevLett.126.208102, which includes Refs. [26–30], for details of the approximation, calculations for run-and-tumble particles, details of the simulation method, and a comparison with an effective temperature model. Note that we do not consider the effective temperature model [31,32] as an approximation of the activity of the active particle but as an independent nonequilibrium model. Models where particles have different temperatures have recently received much attention [33–36].
[26] K. Kaneko, Adiabatic elimination by the eigenfunction expansion method, Prog. Theor. Phys. **66**, 129 (1981).
[27] J. Tailleur and M. E. Cates, Sedimentation, trapping, and rectification of dilute bacteria, Europhys. Lett. **86**, 60002 (2009).
[28] A. Baskaran and M. C. Marchetti, Hydrodynamics of self-propelled hard rods, Phys. Rev. E **77**, 011920 (2008).
[29] P.-G. De Gennes and J. Prost, *The Physics of Liquid Crystals* (Oxford University Press, New York, 1993), Vol. 83.

[30] H. Risken, *Fokker-Planck Equation* (Springer, New York, 1996).
[31] D. Levis and L. Berthier, From single-particle to collective effective temperatures in an active fluid of self-propelled particles, Europhys. Lett. **111**, 60006 (2015).
[32] G. Szamel, Self-propelled particle in an external potential: Existence of an effective temperature, Phys. Rev. E **90**, 012111 (2014).
[33] A. Y. Grosberg and J.-F. Joanny, Nonequilibrium statistical mechanics of mixtures of particles in contact with different thermostats, Phys. Rev. E **92**, 032118 (2015).
[34] S. N. Weber, C. A. Weber, and E. Frey, Binary Mixtures of Particles with different Diffusivities Demix, Phys. Rev. Lett. **116**, 058301 (2016).
[35] E. Ilker and J.-F. Joanny, Phase separation and nucleation in mixtures of particles with different temperatures, Phys. Rev. Research **2**, 023200 (2020).
[36] M. Wang and A. Y. Grosberg, Three-body problem for Langevin dynamics with different temperatures, Phys. Rev. E **101**, 032131 (2020).
[37] A Iniesta and J. G. de la Torre, A second-order algorithm for the simulation of the Brownian dynamics of macromolecular models, J. Chem. Phys. **92**, 2015 (1990).
[38] K. V. Klenin, H. Merlitz, and J. Langowski, A Brownian dynamics program for the simulation of linear and circular dna and other wormlike chain polyelectrolytes, Biophys. J. **74**, 780 (1998).
[39] J. D. Weeks, D. Chandler, and H. C. Anderson, Role of repulsive forces in determining the equilibrium structure of simple liquids, J. Chem. Phys. **54**, 5237 (1971).
[40] J. Elgeti and G. Gompper, Wall accumulation of self-propelled spheres, Europhys. Lett. **101**, 48003 (2013).
[41] J. Elgeti and G. Gompper, Run-and-tumble dynamics of self-propelled particles in confinement, Europhys. Lett. **109**, 58003 (2015).
[42] M. Born and R. Oppenheimer, Zur quantentheorie der molekeln, Ann. Phys. (Leipzig) **389**, 457 (1927).
[43] J. A. Kromer, N. de la Cruz, and B. M. Friedrich, Chemokinetic Scattering, Trapping, and Avoidance of Active Brownian Particles, Phys. Rev. Lett. **124**, 118101 (2020).
[44] M. E. Cates, Diffusive transport without detailed balance in motile bacteria: Does microbiology need statistical physics?, Rep. Prog. Phys. **75**, 042601 (2012).
[45] C. Lozano, B. ten Hagen, H. Löwen, and C. Bechinger, Phototaxis of synthetic microswimmers in optical landscapes, Nat. Commun. **7**, 12828 (2016).
[46] C. Lozano and C. Bechinger, Diffusing wave paradox of phototactic particles in traveling light pulses, Nat. Commun. **10**, 2495 (2019).
[47] A. Kaiser, S. Babel, B. ten Hagen, C. von Ferber, and H. Löwen, How does a flexible chain of active particles swell?, J. Chem. Phys. **142**, 124905 (2015).
[48] R. G. Winkler and G. Gompper, The physics of active polymers and filaments, J. Chem. Phys. **153**, 040901 (2020).
[49] J. Tailleur and M. E. Cates, Statistical Mechanics of Interacting Run-and-Tumble Bacteria, Phys. Rev. Lett. **100**, 218103 (2008).
[50] É. Fodor, C. Nardini, M. E. Cates, J. Tailleur, P. Visco, and F. van Wijland, How Far from Equilibrium is Active Matter?, Phys. Rev. Lett. **117**, 038103 (2016).
[51] D. Martin, J. O'Byrne, M. E. Cates, É. Fodor, C. Nardini, J. Tailleur, and F. van Wijland, Statistical mechanics of active Ornstein-Uhlenbeck particles, Phys. Rev. E **103**, 032607 (2021).
[52] B. Liebchen and H. Löwen, Synthetic chemotaxis and collective behavior in active matter, Acc. Chem. Res. **51**, 2982 (2018).
[53] S. Saha, R. Golestanian, and S. Ramaswamy, Clusters, asters, and collective oscillations in chemotactic colloids, Phys. Rev. E **89**, 062316 (2014).
[54] O. Pohl and H. Stark, Dynamic Clustering and Chemotactic Collapse of Self-Phoretic Active Particles, Phys. Rev. Lett. **112**, 238303 (2014).
[55] B. Nasouri and R. Golestanian, Exact Phoretic Interaction of Two Chemically Active Particles, Phys. Rev. Lett. **124**, 168003 (2020).